



# A new control parameter to predict micro-warping-induced job failure in LPBF of Ti6Al4V titanium alloy

Gianluca Buffa<sup>1</sup> · Antonio Costa<sup>2</sup> · Dina Palmeri<sup>1</sup> · Gaetano Pollara<sup>1</sup> · Antonio Barcellona<sup>1</sup> · Livan Fratini<sup>1</sup>

Received: 3 January 2023 / Accepted: 26 February 2023  
© The Author(s) 2023

## Abstract

Laser powder bed fusion (LPBF) includes a few printing techniques widely used, in recent years, concerning the additive manufacturing of Ti6Al4V alloys. These produced parts, typically utilized in sectors such as aerospace and biomedical, are characterized by very high added value. It is therefore fundamental to identify the influence of process parameters typical of LPBF technology on the occurrence of warping leading to process failure. This study deals with the characterization of single-track and “micro-scale” level warping phenomena which may lead to protrusion of material over the powder bed and process failure before normal termination. This phenomenon was investigated as a function of process parameters, referring also to the strength and ductility characteristics of the manufactured samples. With this purpose, several samples were printed using variable process parameters both in terms of line energy density (LED) values and in terms of laser power and speed combinations such as to guarantee constant LED values. For the samples that did not show significant micro-warping phenomena, in addition to the transversal and longitudinal geometric characterization of the single track, tensile tests were performed to determine both the resistance of the material and the ductility characteristics. The single tracks, for given process parameters, were printed on a homogeneous material substrate. For every single track, a microstructural and morphological transverse and longitudinal characterization has been carried out and the measured geometrical features were correlated to the process parameters. The obtained results allowed the identification of a new threshold parameter, indicating the limit operating conditions beyond which significant warping phenomena and process failure occur.

**Keywords** Laser powder bed fusion · Ti6Al4V · Warping · Additive manufacturing

## 1 Introduction

In the last 10 years, a progressive increase in studies concerning additive manufacturing has been observed, with specific reference to the techniques used for the optimization of process parameters. Numerous studies refer to the maximization of the resistance and functional characteristics of manufactured products [1, 2]. Laser powder bed fusion (LPBF) is an additive manufacturing technique where the part is fabricated layer by layer starting from metallic powder. For each layer, the powder is selectively melted by a laser energy source following an assigned path. In this way, it is possible

to produce complex geometries without any restrictions and reduce lead time and waste. For these reasons, LPBF is widely used for aerospace, automotive, and biomedical applications [3] where lightweight structures with complex shapes are often requested. In the aforementioned sectors, in which there has been a rapid diffusion of additive manufacturing technologies, the most used material is the Ti6Al4V alloy which allows the creation of highly resistant and low-weight components, as well as components characterized by high biocompatibility. Despite these advantages, there are some issues related to the process. The wrong choice of process parameters can lead to several defects, such as gas porosity, lack of fusion, balling, residual stress, distortion, and warping which can affect the mechanical properties and the quality of the final part. Luo et al. [4] studied the conditions that promote the keyhole defect formation in a selective laser melted beta titanium alloy, while Singla et al. [5] collected in their study the main research that highlighted the main defects found in the selective laser melting

✉ Gianluca Buffa  
gianluca.buffa@unipa.it

<sup>1</sup> Department of Engineering, University of Palermo, Viale Delle Scienze, 90128 Palermo, Italy

<sup>2</sup> DICAR Department, University of Catania, Viale Andrea Doria 6, 9515 Catania, Italy

process. Zhou et al. [6] studied the mechanism of porosity formation during the selective laser melting process by correlating it with the kinetic characteristics of the melt pool as a function of process parameters. Additionally, as reported by Stavropoulos et al. [7], residual stresses arise due to the rapid heating and cooling cycle during the process, and they play a fundamental role in dimensional accuracy limiting the application of the produced components. Hence, producing parts with low or neglectable residual stress is one of the fundamental challenges in LPBF processes. As indicated in the study of Mugwagwa et al. [8], this is because residual stresses can lead to part distortion when the sample is removed from the base plate or even, considering the findings of Clijsters et al. [9], to job failure during the printing when residual stresses are too large. The residual stress mechanism formation in selective laser melting is the following: first, the newly deposited layer, scanned with the heat source, tends to expand while the underlying solidified material contrasts this expansion, resulting in compressive stress for the new layer and tensile stress for the underlying part. Then, from the study of Mercelis and Kruth [10], it is inferred that, when the heat source is removed, the new layer tends to shrink hampered by the underlying part, resulting in tensile stress for the new layer and compressive stress in the material below. As indicated by Stavropoulos et al. [7], the occurring distortion phenomenon, taking place in every layer due to non-uniform thermal stress, is called warping.

A few papers can be found in the literature focusing on residual stress and warping in SLM processes. Wang et al. [11] investigated the occurrence of warping for overhanging surfaces related to building orientation, scan speed, and laser power. They noted that for low values of building orientation and scan speed, the warping defect will occur more readily. Also, for higher values of laser power, the warping effect will be more evident. Furthermore, for fixed angles of the overhanging surface, only the energy input can be changed to avoid warping defects. On the other hand, if laser power and scan speed are determined to guarantee high part density, the only way to ensure the part quality is to change the inclined angle of the overhanging surface during the designing phase. Calignano [12] also analyzed the occurrence of the warping phenomenon for overhanging structures. In their paper, the importance of the part orientation and the support design phase was highlighted as warp occurs when the laser scans directly on the powder resulting in insufficient anchoring and lifting of the deposited layer. Bugatti et al. [13] studied the effect of overhanging surfaces on the formation of internal defects in the laser powder bed fusion-type process. Lu et al. [14] assessed the warping for thin-walled structures that are widely used for aeronautical applications. They found that different geometrical characteristics, i.e., the wall thickness, the build height, the wall curvature, and the presence of an open or closed structure, play a key role in the warping occurrence. In detail, thicker structures have a beneficial effect while thinner

and higher structures with an accentuated curvature as well as open structures promote warpage.

Moreover, it has been found that the track morphology also plays a crucial role in residual stress magnitude in additively produced parts, being the remelting zone the most critical one for its occurrence. In this regard, [15, 16] studied the structure of single tracks of 24CrNiMo steel selective laser melted. A few studies can be found in the literature in which the track morphology is correlated to the process parameters. Bai et al. [17] investigated the influence of process parameters on the morphology of the melt pool and the surface of each deposited layer of 18Ni300 maraging steel and they highlighted that the surface quality and tensile property are better for an increase of Volume Energy Density.

Wang et al. [18] evaluated, for maraging steel, the process parameters influence on single-track and single-layer SLM experiments. They found that higher laser power and lower scanning speed promote the formation of inclusions, pores, and cracks in the next layers. Yang et al. [19] investigated the influence of laser power, scanning speed, and layer thickness on the height, depth, and width of molten pools. They found that scanning speed is the most influential followed by laser power and layer thickness, having the latter a negligible effect on the track morphology. Additionally, it was noted that the width and the depth of the track increase with increasing laser power while decrease with increasing scanning speed. Gusarov et al. [20] stated that the scanning speed has a relevant effect on the track quality. For fixed laser power, decreasing scan speed leads to a higher width of the melt pool that stabilizes the scan track. Shrestha and Chou [21] analyzed the effect of two different values of line energy density (0.48 J/mm and 0.75 J/mm) on the single-track morphology by using different combinations of laser power and scanning speed. It was noticed that laser power is more influential on the depth size of the single track concerning scanning speed.

It can be noted that, in the above-described papers, the warping phenomenon was mostly studied for overhang structures. Warping was directly correlated to process parameters with particular reference to energy density and building orientation. On the other hand, papers focusing on track morphology allowed the identification of a correspondence between process parameters and track features. It should also be highlighted that the warping phenomena most frequently studied in the literature are macro-scale deformations which, therefore, are strongly influenced by sample size and are more relevant in larger sample sizes. However, warping phenomena may occur on a micro-scale at the deposition of each individual track. Micro-scale warping phenomena are related to the success of the printing process. In fact, when the warpage results in the protrusion of the current layer out of the powder bed, the recoater may get damaged and the printing process fails. Although the deposition of material

that considers multiple tracks, both side-by-side and stacked, determines an overall warping of the component, the morphology of the single track plays a key role when dealing with the study of warping phenomena at the micro-scale. In this way, as reported by the study of Kruth et al. [22] concerning the selective laser melting of an iron-based alloy, the geometry of the single track influences micro-scale warping in both side-by-side and stacked multiple depositions.

A comprehensive direct correlation between the track morphology and the occurrence of the warping phenomenon is still missing in the literature. Additionally, there is no paper focusing on the effect of process parameters on warping and track morphology when a given energy density is assigned. Concerning the energy density, Gong et al. [23] and Song et al. [24] showed that the optimal process parameters are bounded by a minimum and a maximum value of uniform energy density. In addition to this, previous experimental tests by some of the authors [25] have pointed out that, even for uniform energy density values within the optimum zone indicated in the literature, micro-warping phenomena occur in some cases, leading to failure of the printing process.

The optical control system, normally used to control the manufacture of every single layer, has a detection sensitivity of micro-defects which depends on the setting of two threshold values, one referring to the number of errors present in each layer and the other referred to the cumulative surface extension of the defects in each layer. If there are a large number of pieces on the printing platform, it is necessary to raise the two threshold values previously indicated to avoid interruptions of the printing process which are not actually caused by deposition defects of the single layer. In these cases, it is useful to consider a control parameter that guarantees the uniformity of deposition of each layer even in the case in which the control thresholds of the optical system are increased in order to avoid interruptions of the printing process.

In this paper, a new analytical indicator, called “warping alert,” was established with the aim to predict the occurrence of micro-warping phenomena that, in the subsequent stacking of the individual layers, result in the failure of the printing process. A fundamental transverse and longitudinal characterization of the single track obtained the LPBF of Ti6Al4V titanium alloy was carried out with varying scanning speed and laser power. Different sets of process parameters were investigated and a link between the measured geometrical features of the track and the process parameters was established. In addition, the main factors influencing the occurrence of the warping phenomenon have been identified. The produced samples for which excessive warping did not cause the failure of the process were characterized also in terms of mechanical properties. Finally, a process window was obtained, showing the transition from the no-warping

(safe) zone to the warping zone as a function of the process parameters, allowing the identification in the plane  $P_v$  (laser power, scanning speed) of the limit operating conditions to avoid the job failure. The specific experimental plan that has been defined limits the validity of the experimental results obtained to the chosen building orientation and material. Additional results are going to be added in the future in order to broaden the ranges of considered process parameters and materials.

## 2 Methodology

All the experiments were run on an SLM 280HL machine. Ti6Al4V spherical powder (Fig. 1), provided by SLM Solution AG Group, with a particle size distribution of 20–63  $\mu\text{m}$  was used in this study.

A preliminary experimental campaign was carried out using constant scan strategy ( $0^\circ$ ), hatch spacing (120  $\mu\text{m}$ ) and layer thickness (30  $\mu\text{m}$ ), and three different line energy density (LED) values, namely 0.15 J/mm, 0.22 J/mm, and 0.32 J/mm. While the samples with the lowest and the higher value of LED were successfully completed, a failure was detected for the sample with LED equal to 0.22 J/mm. It is worth noting that this value of LED is similar to the one recommended by SLM Solution AG Group, according to which optimal LED is equal to 0.25 J/mm.

In order to investigate the reasons for the observed part failure, five tensile test samples characterized by the same LED and obtained by different combinations of laser power

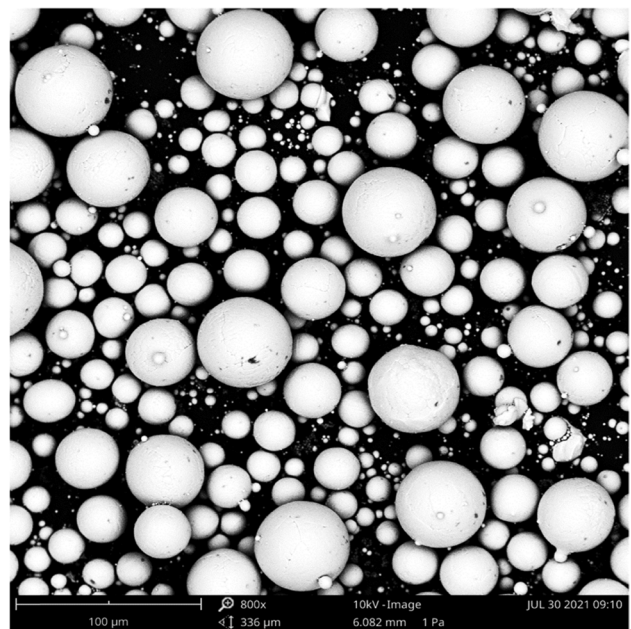


Fig. 1 Ti6Al4V spherical powder provided by SLM Solution

(P) and scan speed ( $v$ ) were built. The tensile test specimens were fabricated as a reduction of the Standard ASTM/E8 with a rectangular cross-Sect. ( $10 \times 4$  mm) and a useful gauge length equal to 22 mm. The process parameters utilized for this experimental study are indicated in Table 1.

Each set of process parameters was associated with an ID number, shown in the first column of Table 1, which was subsequently used to identify the samples. Scan strategy, layer thickness, and hatch spacing were kept constant and equal to  $0^\circ$ ,  $30 \mu\text{m}$ , and  $120 \mu\text{m}$ , respectively, for all the samples.

Quasi-static tensile tests were performed on a Galdabini universal testing machine for the dog bone-shaped specimens with a loading speed of 1 mm/min. Moreover, cube specimens ( $10 \times 10 \times 5$  mm), built with the optimal process parameters provided by SLM Solution ( $P = 350$  W and  $v = 1400$  mm/s) were fabricated and used as substrate for the scanning of single tracks (Fig. 2). The process parameters used for the single tracks were the same P and  $v$  used for the tensile test specimens and indicated in Table 1.

For each process parameter, two cube specimens and three tensile test samples were fabricated. For each cube, four single tracks, extending along the entire length of the cube, were scanned on the last layer of the cube itself, using an assigned P and  $v$ . In Fig. 3, a picture of one of the platforms with the produced samples is shown.

The single tracks were scanned to investigate the effect of the process parameters on the track morphology and, as a consequence, on the final part. One set of cube specimen was used for the metallurgical analysis, while the other one for the SEM analysis.

Each single track was characterized both transversely and longitudinally. For transverse morphology characterization, the melt pool size width (W), depth (D), and height (H) of the single track were observed by Olympus optical microscope

**Table 1** Process parameters were used for this study (samples that showed significant warping phenomena during the printing process are marked in light gray)

	P [W]	$v$ [mm/s]	LED [J/mm]
1	260	1700	0.15
2	380	1700	0.22
3	320	1000	0.32
4	200	895	0.22
5	250	1118	0.22
6	300	1342	0.22
7	350	1566	0.22
8	400	1789	0.22

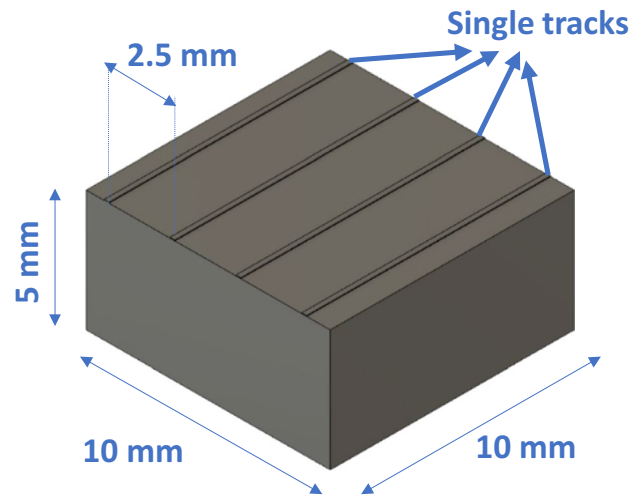


**Fig. 2** Sketch of the cube sample with the single tracks scanned on the last layer

(Fig. 4). For the metallurgical analysis, mounting, grinding, and polishing operations were carried out to prepare the samples to the chemical etching with Kroll's reagent for 45 s to reveal the microstructure and highlight the melt pool zone.

The utilized values of W, D, and H, for each process condition, were determined by mathematically averaging the measurement results of the three single tracks scanned on each cube specimen. Moreover, the area of the melt pool on the substrate (AD), also called remelting zone, and the upper zone (AH) were measured (see again Fig. 4), while a factor F was determined as the ratio between AH end AD.

For the track longitudinal characterization, the top surface of the cube specimens was observed by Phenom ProX Desktop SEM microscope. In this way, it was possible to recreate the entire single track and to observe defects, e.g., necking, which can influence the continuity of the melt pool.

The reconstruction of the single tracks was used to measure the width of the necking zone (N), and the width of the regular zone (L) and to evaluate the L and N parameters averaged along the track.

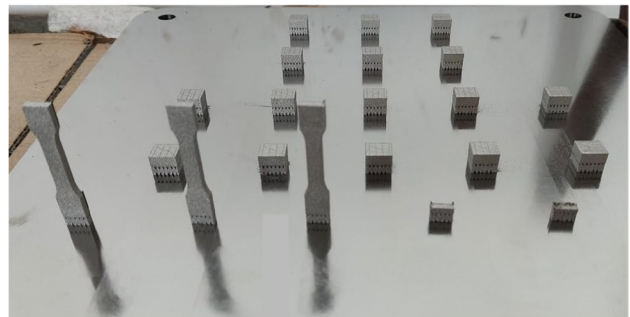


**Fig. 3** Build platform with tensile test and cube specimens

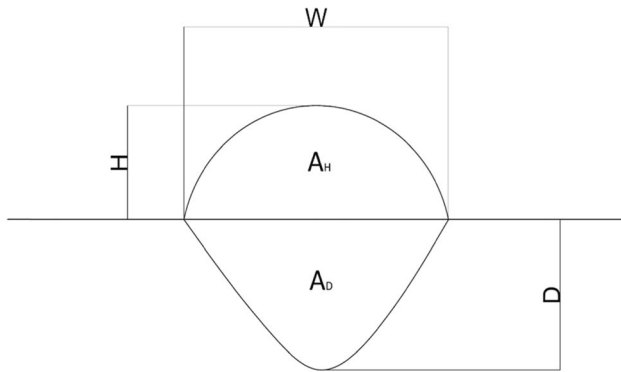


**Fig. 4** Schematic representation of the transversal section of melt pool geometry

In addition, the squareness factor ( $AL/L'$ ) of the longitudinal surface of the single trace ( $AL$ ) was also measured for the chosen reference length ( $L'$ ) of  $9030 \mu\text{m}$ .

### 3 Results and discussion

#### 3.1 Single-track transversal characterization

The transversal characterization of the single tracks for case studies 1 to 8 was carried out by measuring the  $W$ ,  $H$ , and  $D$  parameters of the cross-sections of the three different tracks.

The micrographs acquired in the cross-sections of the samples allowed to identify the remelting zones of the tracks in the substrate, due both to the substrate building and to the single track, as highlighted in Fig. 5. After the identification of the remelting boundary of the single track, the surface extent of the remelting zone (yellow profile) and the unremelted zone (green profile) of the single track itself was evaluated. The average values of the above parameters were obtained for each set of process parameters. A similar procedure was used to determine the average values of parameters  $A_H$  and  $A_D$  and the related parameter  $F$ . It is worth noting that using the average values of the morphological parameters allows taking into account the variability of the parameters between different tracks made with the same process parameters. The results of the morphological characterization of the single tracks as the process parameters varied are shown in Fig. 6. To determine the link between process parameters, average transverse morphology of the single track, and the occurrence of significant warping phenomena, the average values of the measured parameters have been plotted in relation to each set of process parameters. The trends obtained, depicted in Fig. 6, show in abscissa the identification number of the sample, from 1 to 8, to which a given set of process parameters is related.

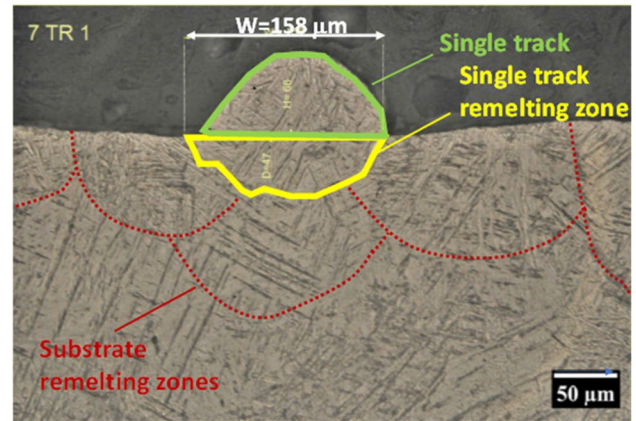


**Fig. 5** Micrograph of the single track for case study 7, first track: identification of the different remelting zones

Concerning  $H$ , which indicates how much the single track emerges from the already deposited substrate, the obtained results show that it assumes higher values for the operating parameters corresponding to the samples which presented significant warping phenomena, i.e., samples 2, 7, and 8. The trend of the parameter  $H$  indicates that there is no direct correlation between the value of  $LED$  and the value of  $H$ . In fact, with the same value of  $LED$  (IDs 2, 4–8), the values of  $H$  vary significantly. To better understand the obtained result, it is necessary to highlight that the laser power value  $P$  is directly related to the temperature gradient established in the molten material during the deposition of the single track, while the scanning speed influences the interaction time of the laser with a given portion of the material.

As the laser power increases, the temperature reached by the melted material increases, thus resulting in decreasing viscosity. In addition to this, the increase of the  $P$  parameter also determines, other parameters being equal, an increase in the portion of melted material of the material substrate on which the single track is deposited. Therefore, in general, increasing values of  $P$ , other parameters being equal, result in increasing  $D$ . The described trend was also obtained by Balbaa et al. [26] who investigated the effect of process parameters on the morphology of a single track of selective laser melted Inconel 718. The same trend was highlighted by Yadroitsava et al. [27] that studied the single tracks of SLM Ti6Al4V. In turn, the effect of increasing scanning speed on the viscosity and thermal gradient characteristics of the melt pool during the deposition of each single track is the opposite. Increasing scanning speed corresponds to a shorter laser exposure time of the material and therefore increasing speeds result in decreasing  $D$  values. In addition, it should be noted that the combined effect of high laser power and scanning speed activates axial flows of material, Marangoni type, due to the reduced viscosity of the molten material, in the opposite direction with respect to the one of the laser scanning,

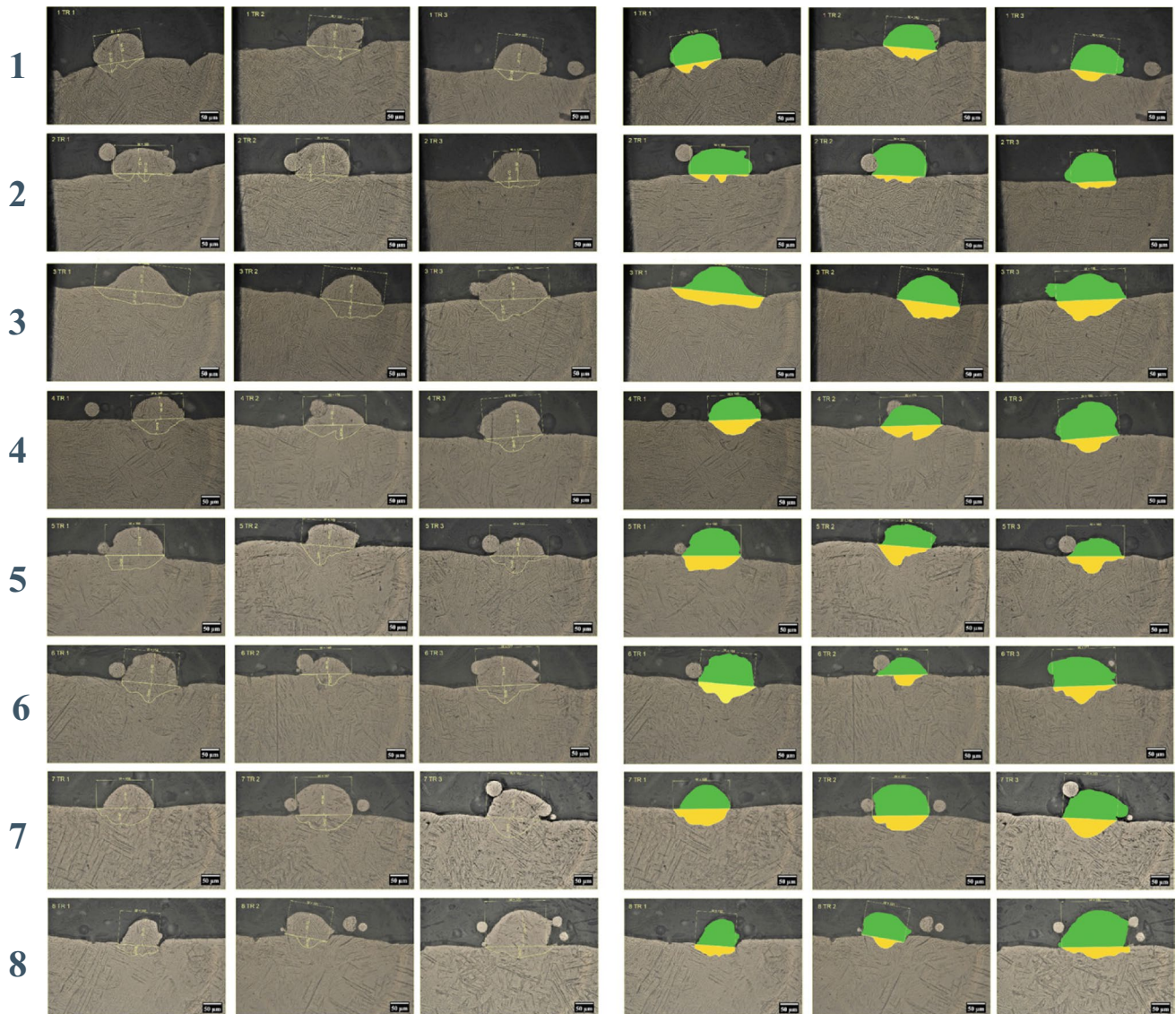
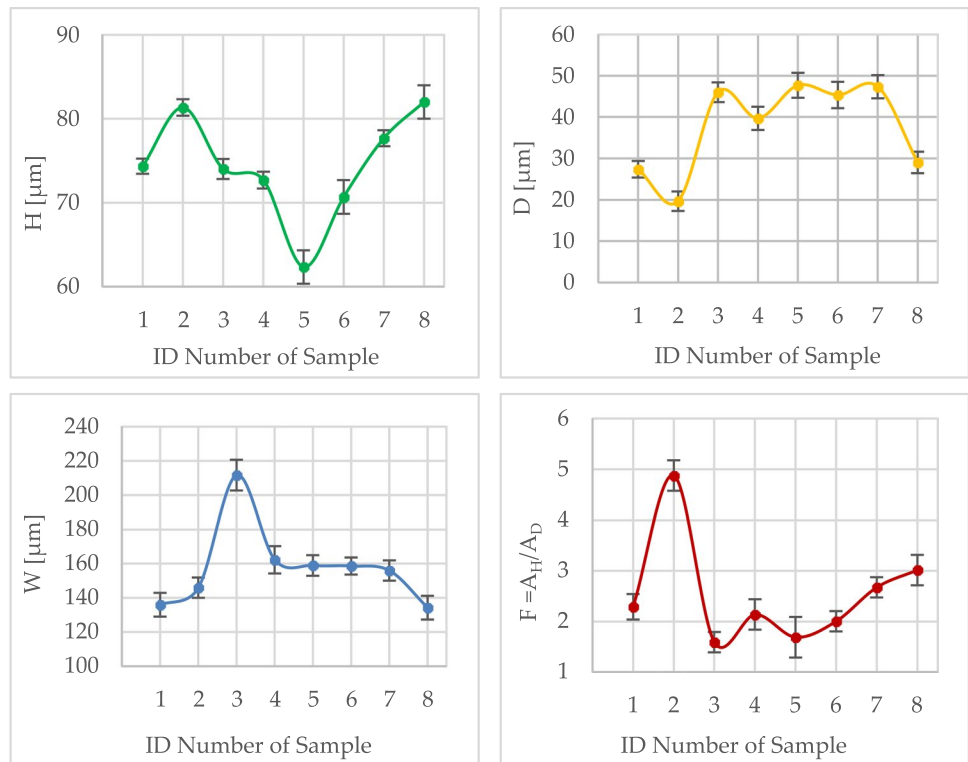


**Fig. 6** Morphological transversal characterization of the three single tracks for each case study (1–8). Measuring of  $W$ ,  $D$ , and  $H$  parameters and highlighting of the  $A_H$  (green) and  $A_D$  (yellow) surfaces

resulting in a protrusion of the deposited track that can give rise to an increase of  $H$ . The latter phenomenon is known in the literature as Lu et al. [28] studied the morphology of the molten pool by correlating different configurations to the process parameters. Qiu et al. [29] studied the melt pool characteristics related to the surface structure of selective laser melted samples while Yin et al. [30] showed the correlation between different melt pool configurations and spatter formation dynamics during single-track deposition. Zhang et al. [31] studied the melt pool morphology using a simulation model. The morphological parameters characterizing the single tracks, shown in Fig. 7, highlight two different trends. The first trend is observed for the parameters  $H$  and  $F$ , for which it is visible the absence of a significant single

effect related to the value of laser power and scanning speed. In fact, for these parameters, there is no correlation with the combined value of  $P$  and  $v$  expressed by the LED parameter. Instead, an increase in the values of  $F$  and  $H$  was observed for the samples that have shown significant warping phenomena. These trends, considering the influence of the parameters  $P$  and  $v$  on temperature, thermal gradients, and kinetics of the molten material, during the single-track deposition process, denote that for particular combinations of high  $P$  and  $v$ , the kinetics of the molten material coupled with the high thermal gradients can result in the formation of a track protrusion in the area behind the laser scan that stabilizes as the track cools and results in high  $H$  and  $F$  values. The second trend is the one found for the  $W$  and  $D$  parameters.

**Fig. 7** Influence of process parameters on the morphological parameters that characterize the transversal single track. 2, 7, and 8 are the process conditions that generate warping phenomena



It is observed that the width of the track and the depth of the track in the deposition substrate are significantly affected by high scanning speeds. When scanning speeds exceed 1700 m/min, the above parameters assume decreasing values.

### 3.2 Single-track longitudinal characterization

The longitudinal morphological characterization allowed the study of the variability of the track geometrical parameters along the track itself, for each set of process parameters. The measurements taken are shown in Fig. 8 for the second track of all the case studies. In addition to the average values of the morphological parameters along the single-track L and N, the overall area occupied by the single track for the chosen reference length  $L'$  of 9030  $\mu\text{m}$  was measured.

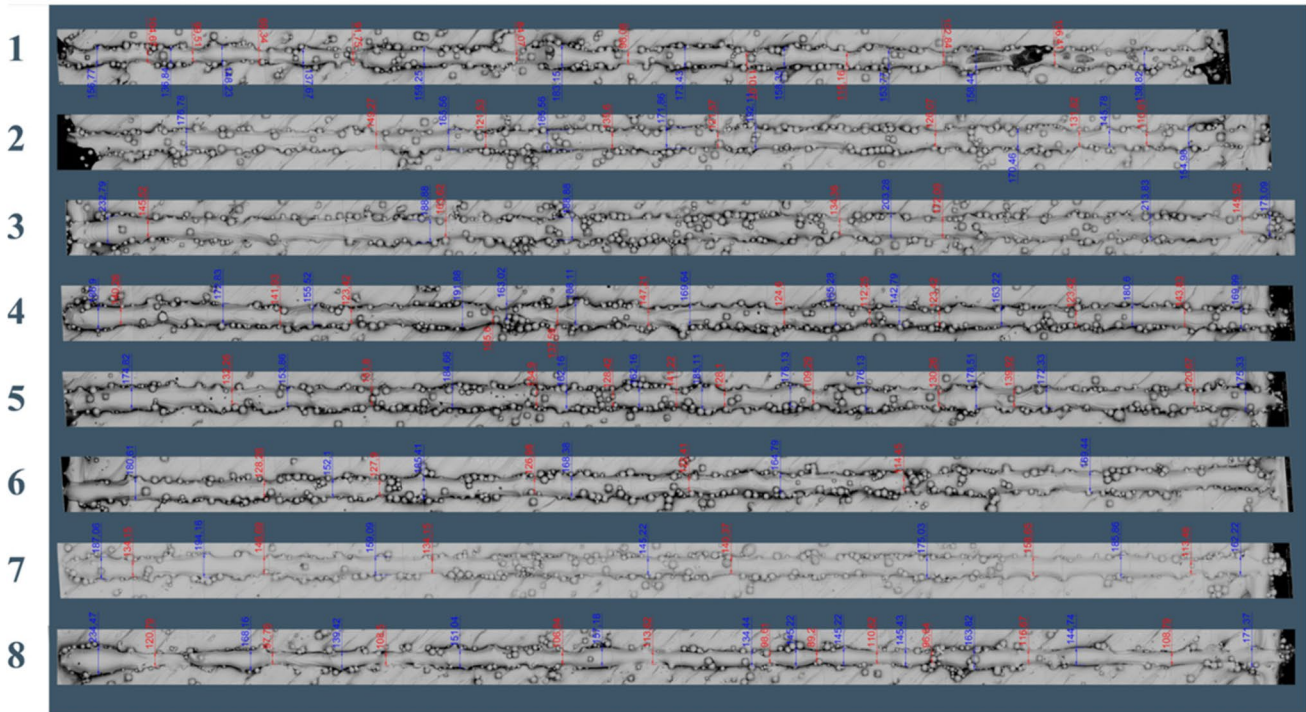
Figure 9 shows the measurement of the AL parameter as the process parameters change, while the numerical values of the squareness factor  $AL/L'$  and of the L and N values averaged along the track are shown in Fig. 10.

Also in this case, the visualization of the longitudinal morphological parameters of the track, as the process conditions vary, showed a trend consistent with the ones already observed during the transverse characterization of the tracks. In particular, the L parameter showed a trend analogous to the one found for the W parameter. This analogy suggests that the influence of process parameters

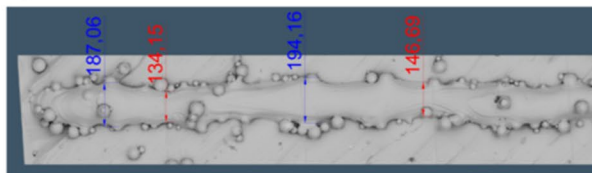
on the width of the single track is not affected by variability phenomena either along the same track or associated with the execution of adjacent tracks with the same process parameters. In other words, the analogous transversal and longitudinal trends of the parameters W and L allow to highlight that the width of the track is not a parameter correlated to the onset of warping phenomena despite its variability both longitudinally, for a given track, and between different tracks. The observations and experimental measurements performed, both considering different cross-sections of the tracks, and carrying out the longitudinal measurements of the different tracks made with the same process parameters, have confirmed the repeatability of the described trends. A trend similar to the one found for L and W was observed also for the  $A_L/L'$  parameter, indicating that the parameters identified to define the transverse section can be effectively used for the track characterization, being the variability over the track length limited. For these parameters, increasing values of LED result, in general, in increasing values of the parameters related to the track width, i.e., W and L. It should also be noted that, in all the previous graphs, the error bars of the measurements make the results obtained consistent as they do not cause overlaps and interferences that modify the main results highlighted.

For large scanning speed values, the effect of speed prevails over the one of LED, resulting in a reduction of W and L. As the H parameter is regarded, increasing values

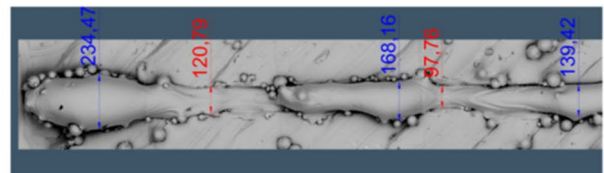
a)



b)



Sample 7



Sample 8

**Fig. 8** (a) Longitudinal characterization of the single track and (b) magnification of the initial part of the track for the samples 7 and 8. Measurement of L (blue) and N (red) are highlighted

of H are found as LED increases, although at constant LED (0.22 J/mm), H decreases for scan speed values that exceed 1700 mm/s. In this way, it can be stated that the longitudinal parameters are not significantly affected by the process conditions that give rise to the warping phenomena.

### 3.3 Mechanical characterization

First of all, it is noted that the process parameters used for printing the samples corresponding to case studies 2, 7, and 8 led to significant warping phenomena during the process and therefore it was not possible to produce the specimens to be used for the tensile tests. The mechanical characterization tests carried out on the samples made with the process parameters that did not give rise to warping phenomena are shown in Fig. 11. Considering the UTS resistance values, the most influential parameter

is the ratio between P and v, i.e., the value of the LED parameter. In fact, using the same LED values, although obtained with different combinations of laser power and feed rate, the samples have similar UTS. In particular, for the samples characterized by LED values equal to 0.22 J/mm, which is close to the one recommended by the SLM printer manufacturer for the material considered, the best tensile strength results were obtained, while lower strength values were obtained both for lower LED values (0.15 J/mm) and for higher LED values (0.32 J/mm).

However, a different influence of the process parameters was observed in reference to the ductility of the material measured through the parameter Elongation to Fracture (ETF%). In particular, the results obtained showed that the ETF values increase as the value of P increases, even considering specimens produced with the same LED value. As shown in Fig. 10, the best ETF



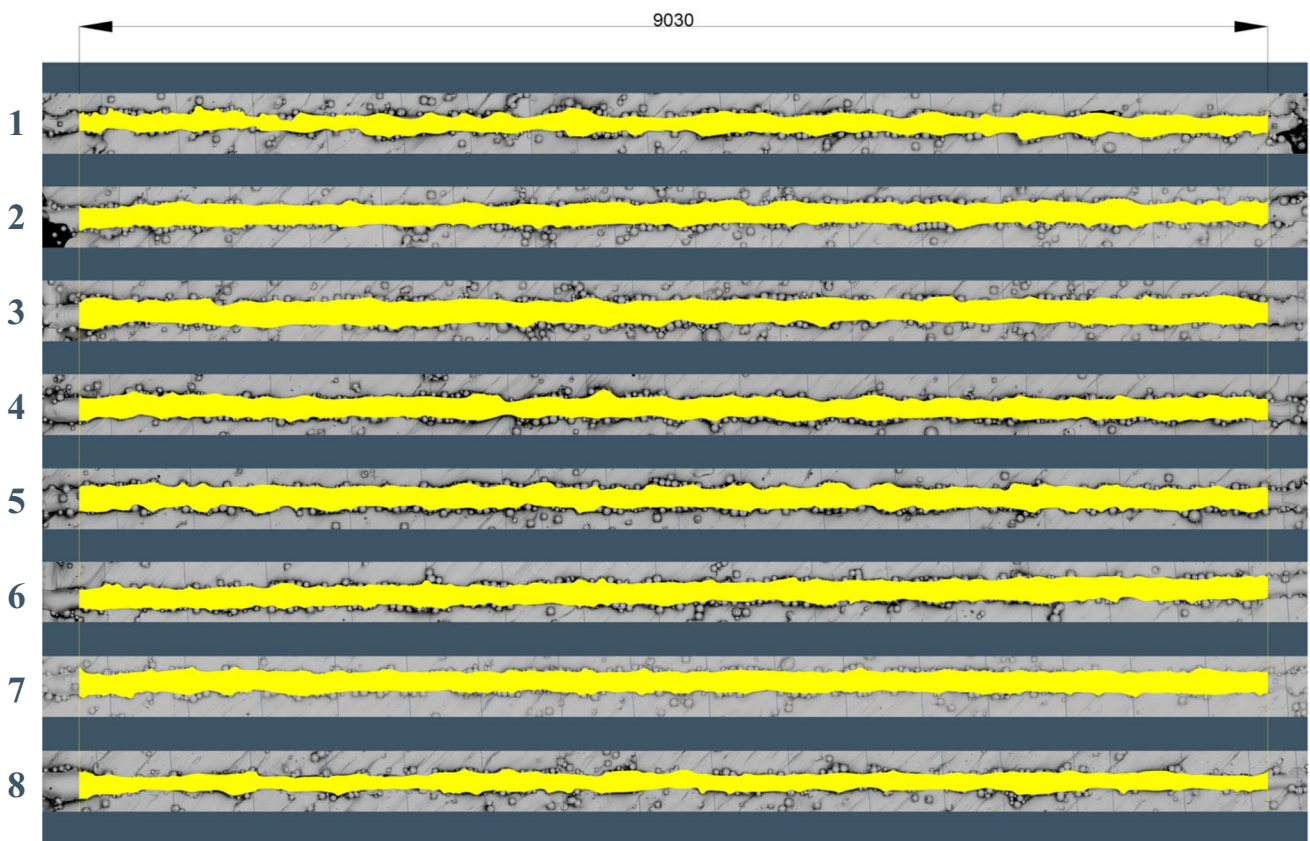


Fig. 9 Measurement of the area occupied by the single track ( $A_L$ ) for the chosen reference length ( $L'$ ) of 9030  $\mu\text{m}$

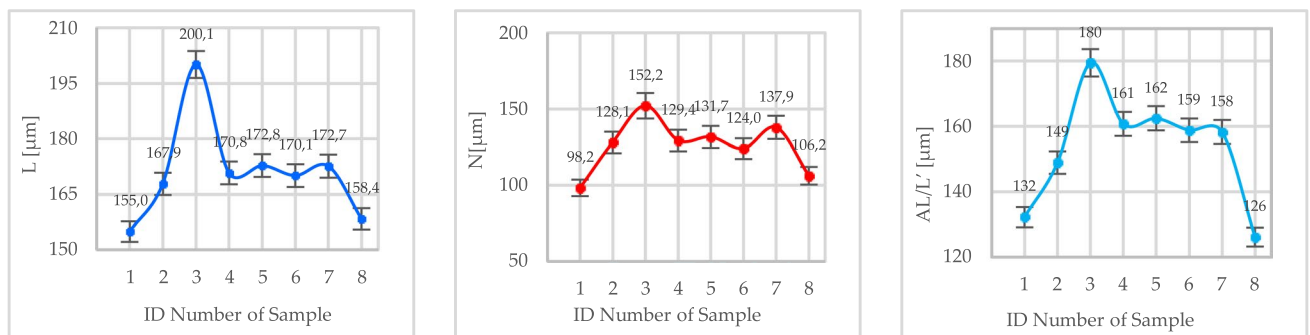


Fig. 10 Longitudinal characterization of the single tracks for the considered case studies. Measurement of  $L$ ,  $N$ , and  $A_L/L'$  parameters

values were obtained for samples made with laser powers of 320 W and 300 W respectively, although the same samples were characterized by different LED values.

### 3.4 Threshold parameter for warping alert

The observation of the positioning of the experimental points within the  $P, v$  plane and the subsequent identification of those that produced significant warping

phenomena allowed to highlight the region of process parameters within which the occurrence of the warping phenomenon occurs.

As shown in Fig. 12, warping phenomena occur in a region of the  $P, v$  plane characterized by simultaneously higher  $P$  and  $v$  values. Points corresponding to process parameters that gave rise to warping phenomena are represented in red.

The results obtained in the morphological characterization steps of the single tracks showed that high  $P$  and  $v$

**Fig. 11** Tensile test results for the samples without warping effect

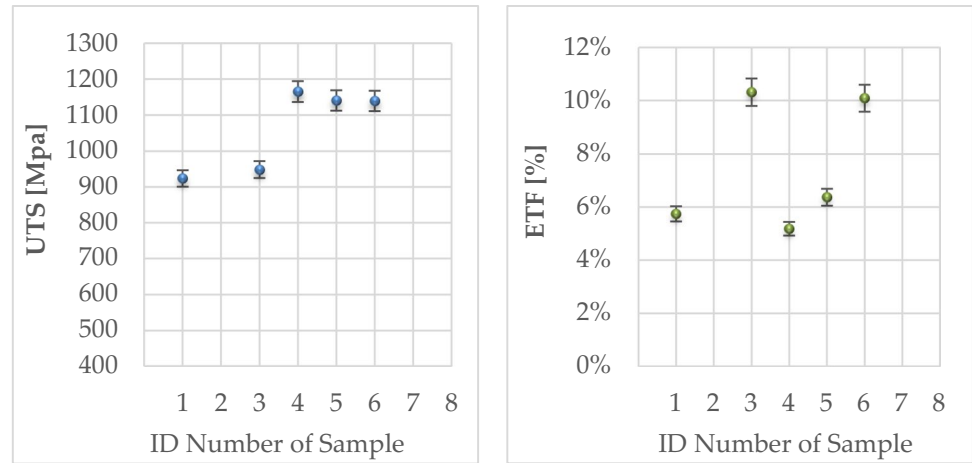
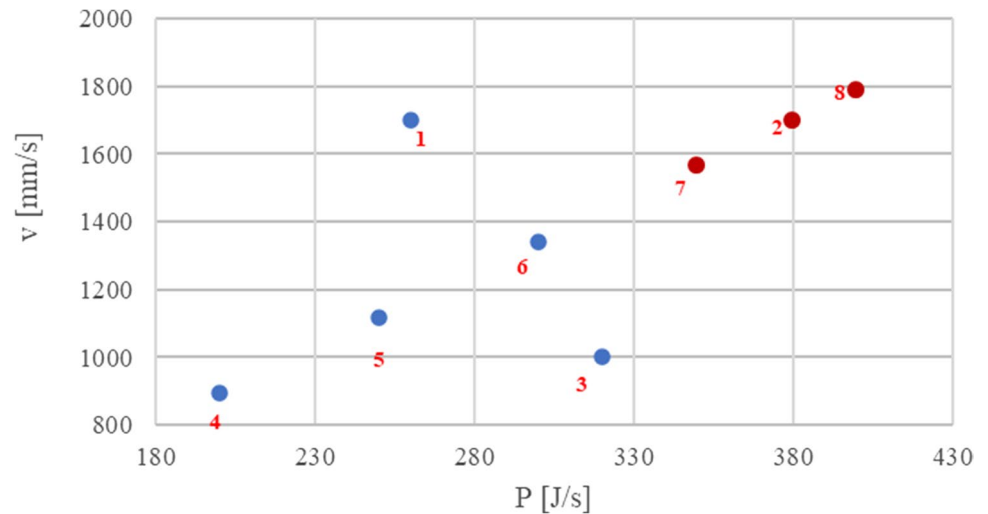


**Fig. 12** Schematic representation of the experimental tests in the P-v plane

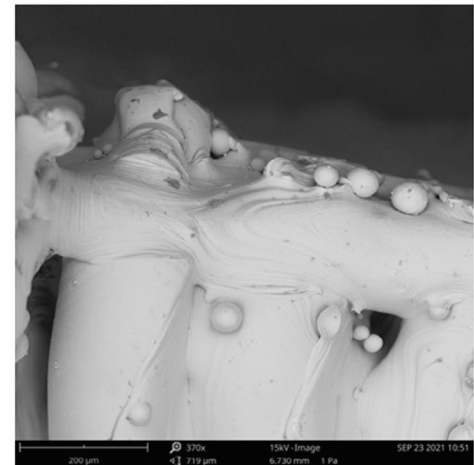
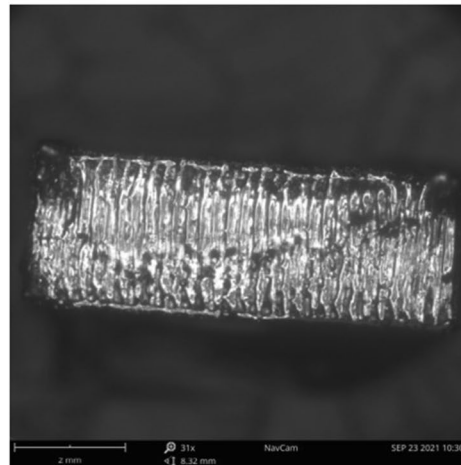


values can lead to warping phenomena when they activate the kinetics of the molten material during the execution of the track and when the cooling rates are such as to stabilize the protrusion conditions of the track in the solid state. The stacking of protrusions does not occur in the central areas of samples because of the lower thermal gradients. Figure 13 shows SEM images, at different magnifications, of the upper surfaces of the specimens corresponding to case studies 7 and 8. The printing process of these samples failed after a few layers because warping phenomena occurred near the edges, resulting in a protrusion of the solidified material over the powder bed surface with consequent recoater damage. It should be observed that a safety optical control system is often present in commercial machines in order to interrupt the process in case of occurrence of these defects, thus preventing serious damage to the machine hardware. However, as it has already been highlighted in the introduction, when the printing area is large with respect to the platform area, i.e., several parts are being printed for a given job, the traditional optical control systems can generate interruption

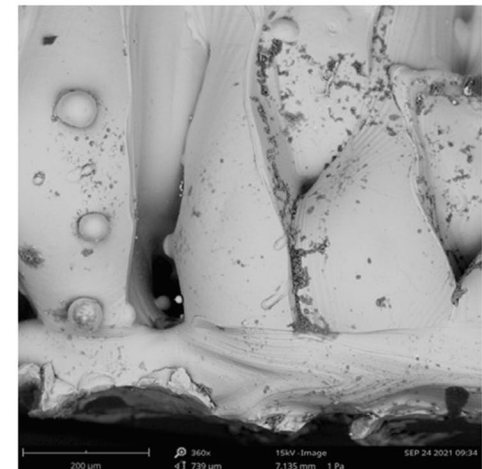
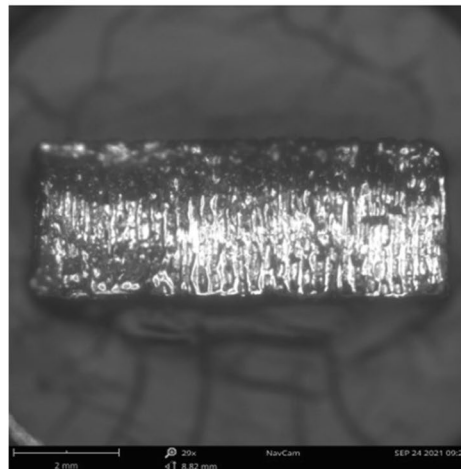
alerts during the printing process even if the deposition morphology of the single layer does not show significant warping phenomena. The choice of the maximum amount of protrusion beyond the new layer tolerated is left to the final user, but usually it hardly exceeds 30 microns. In this study, the above value was considered. Micrographic observations revealed what had already been inferred from the morphological characterization phase of the tracks. Warping accumulates near the edges of the specimen as the overlapping of the layers progresses because the higher cooling rates at end of the tracks, near the edges, promote the stabilization of the track protrusion conditions in the solid state. In subsequent layer overlays, the stacking of the protrusions leads to a rapid drift of the actual geometry of the sample from the designed geometry. The cross-sectional characterization of the single tracks showed that the deformation occurs when both high LED values and high scanning speed, capable of activating the kinetics of liquid phase in the track, are selected. As the melted material is regarded, high LED values lead to higher fluidity, while high scanning speed values lead to

**Fig. 13** Macro and SEM images of the top surface of the failed (a) 7 and (b) 8 case studies. Significant warping visible near the edges

**a) Sample 7 – LED 0.22 J/mm**



**b) Sample 8 – LED 0.22 J/mm**



high kinetics. The coexistence of the two conditions leads to the formation of considerable protrusions at the edges of the tracks. Micro-warping phenomena are therefore associated with the thermal and kinetic conditions of the melted material. The above conditions result in a consequent increase in the H value. The above phenomenon does not occur in the central parts of the tracks because the thermal gradients within the single tracks are mitigated and therefore, in the solidified state, there is only a small increase in the H parameter of the single track. Although LED is a commonly used parameter to identify process conditions in LPBF, especially in industry, experimental observations and morphological characterizations of single tracks suggest that, at a micro-scale level, the warping phenomenon does not occur for a given range of “wrong” LED values. Instead, warping occurs when the combination of laser power value and scan rate value exceeds a threshold value. In these conditions, the reduced viscosity of materials, favored by high laser power and low scanning speed values, i.e., high values of LED,

combines with the high “kinetic energy” of the melted pool, given by high scanning speed and resulting in the axial flows of the material previously observed.

For the samples subjected to morphological and mechanical characterization, a “warping alert” parameter was then established as the combined effect of LED and kinetic energy of the scan. Being LED directly proportional to laser power and inversely proportional to scanning speed while the kinetic energy directly proportional to the square of the scanning speed, the warping alert parameter WA was defined as:

$$WA \sim LED * Kineticenergy \sim \frac{P}{v} * v^2 \tag{1}$$

$$WA = \frac{Pv}{1000} [Jmm/s^2] \tag{2}$$

It was therefore assumed that there can be a threshold value of WA above which warping occurs. To provide

robustness to the above hypothesis, eleven additional samples were printed with process parameters scattered within the P,v plane originally considered. For these additional samples, only the P and v parameters were varied while all other printing parameters were kept constant. The WA parameter was evaluated also for the additional samples, and significant deformation phenomena were reported to occur, leading to the failure of the printing process before completion. The process parameters used for the definition of the eleven new points of the experimental plan have been reported in the following Table 2. In the same table, the samples for which the printing process failed due to warping phenomena have been highlighted in light gray. It is observed that all the samples that showed warping phenomena are characterized by values of WA higher than the value of the same parameter for the samples for which the printing process did not fail. For a better visualization of the new obtained

results, all experimental points, both original and additional, were represented in the P,v plane. Points corresponding to process parameters that gave rise to warping phenomena were represented in red. This full plane is shown in Fig. 14.

In the full plan shown in Fig. 14, two dashed curves characterized by constant WA values and delimiting safe process conditions from warping have been drawn. This value falls in the range between 466 and 506 [Jmm]. It is interesting observing that the mechanical characterization of the samples belonging to the original experimental plan has shown that the best characteristics of strength and ductility are possessed by the sample made with the process parameters of point 6. This means that for given value of LED, that is considering all the points belonging to a given straight line of equation  $P/v = \text{constant}$ , the optimum of the mechanical characteristics is positioned in proximity of the warping alert region.

**Table 2** Process parameters used for this study (1–8) and samples added for the robustness of threshold warping alert parameter (samples that showed significant warping phenomena during the printing process are marked in light gray)

P [W]	v [mm/s]	LED [J/mm]	WA=Pv/1000 [Jmm]	Original experimental plane sample
200	895	0.22	179	4
220	900	0.24	198	
310	900	0.34	279	
250	1118	0.22	280	5
320	1000	0.32	320	3
220	1632	0.13	359	
400	900	0.44	360	
300	1342	0.22	403	6
277	1579	0.18	437	
260	1700	0.15	442	1
280	1632	0.17	457	
220	2120	0.10	466	
310	1632	0.19	506	
350	1566	0.22	548	7
400	1388	0.29	555	
380	1700	0.22	646	2
400	1632	0.25	653	
400	1789	0.22	716	8
400	2120	0.19	848	

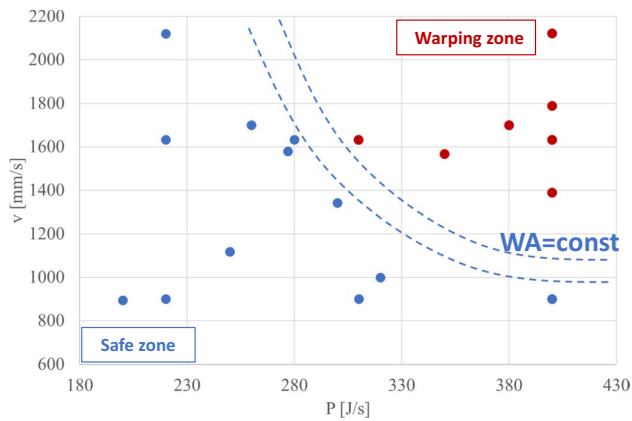


**Fig. 14** Schematic representation of the full experimental tests in the  $P, v$  plane. Dashed curves delimit the range of the WA parameter

## 4 Summary and conclusions

In this work, a new parameter to prevent job failure due to warping was established, and a threshold range was identified through the correlation between the main process parameters used in the LPBF process and the occurrence of “micro-scale” level warping phenomena. To this end, the morphological analysis and quantitative evaluation of the transversal and longitudinal characteristic parameters of the track were carried out together with the mechanical characterization of the samples for which the SLM printing process was successful. The obtained results allow to draw the following main conclusions:

- The study and characterization of the single tracks make possible to identify the track morphological parameters that are related to the occurrence of micro-warping phenomena. The specific contribution of LED and kinetic energy to the occurrence of warping phenomena was also demonstrated.
- The transverse characterization of the single tracks showed that warping occurs when there is a mutual action of the effect produced by high LED values and the effect produced by the scanning speed which, in the case of high values, activates the kinetics of the track in liquid phase that leads to the formation of significant protrusions at the edge of the tracks themselves. Micro-warping phenomena are associated with the thermal and kinetic conditions of the molten material resulting in increased H value.
- The longitudinal characterization of the single tracks showed that, although not perfectly constant conditions are observed in all the tracks, the longitudinal parameters are not significantly affected by the operating conditions that give rise to the warping phenomena.
- The study and characterization of the single tracks made it possible to identify the track morphological parameters

that are related to the occurrence of micro-warping phenomena and the specific contribution of LED and kinetic energy to the occurrence of warping phenomena was also highlighted. It arose that the warping phenomenon is not dependent on the LED parameter only. Instead, it occurs when large values of laser power value and scan rate are used. With reference to the optimal process windows reported in the literature, a new zone called warping alert zone was identified within the optimal process parameter window.

- Micro-warping accumulates near the edges of the specimen as the overlapping of the layers progresses because of the higher cooling rates close to the end of the track, promoting the stabilization of the track protrusion in the solid state. In subsequent layer overlays, the stacking of the protrusions leads to a rapid drift of the actual geometry of the sample from the designed one and process fail before regular termination.
- The mechanical characterization highlighted that the best characteristics of strength and ductility, for a given LED value, are obtained with operating parameters close to the warping alert region in the  $(P, v)$  plane. The value of LED plays a key role in determining the material strength, while ductility is mainly influenced by laser power P.
- The developed analytical model can be used to predict whether the selected values of P and v, although within the window of optimum parameters, will result in job failure because of warpage.

**Author contribution** All authors contributed to the study conception and design. Material preparation and data collection were performed by Dina Palmeri, Gaetano Pollara, and Antonio Barcellona. Data analysis was performed by Dina Palmeri, Livan Fratini, Antonio Costa, and Gianluca Buffa. The first draft of the manuscript was written by Dina Palmeri and all authors commented on previous versions of the manuscript. All authors read and approved the final manuscript.

**Funding** Open access funding provided by Università degli Studi di Palermo within the CRUI-CARE Agreement. This research was carried out with the support of funds from PO FESR Sicilian Region 2014–2020.

## Declarations

**Conflict of interest** The authors declare no competing interests.

**Open Access** This article is licensed under a Creative Commons Attribution 4.0 International License, which permits use, sharing, adaptation, distribution and reproduction in any medium or format, as long as you give appropriate credit to the original author(s) and the source, provide a link to the Creative Commons licence, and indicate if changes were made. The images or other third party material in this article are included in the article's Creative Commons licence, unless indicated otherwise in a credit line to the material. If material is not included in the article's Creative Commons licence and your intended use is not

permitted by statutory regulation or exceeds the permitted use, you will need to obtain permission directly from the copyright holder. To view a copy of this licence, visit <http://creativecommons.org/licenses/by/4.0/>.

## References

- Khosravani MR, Berto F, Ayatollahi MR et al (2022) Characterization of 3D-printed PLA parts with different raster orientations and printing speeds. *Sci Rep* 12:1016. <https://doi.org/10.1038/s41598-022-05005-4>
- Atakok G, Kam M, Koc HB (2022) Tensile, three-point bending and impact strength of 3D printed parts using PLA and recycled PLA filaments: a statistical investigation. *J Mater Sci Technol* 18:1542–1554. <https://doi.org/10.1016/j.jmrt.2022.03.013>
- Aufa AN, Hassan MZ, Ismail Z (2022) Recent advances in Ti-6Al-4V additively manufactured by selective laser melting for biomedical implants: prospect development. *J Alloys Compd* 896:163072. <https://doi.org/10.1016/j.jallcom.2021.163072>
- Luo X et al (2021) Achieving ultrahigh-strength in beta-type titanium alloy by controlling the melt pool mode in selective laser melting. *Mater Sci Eng A* 823(June):141731. <https://doi.org/10.1016/j.msea.2021.141731>
- Singla AK et al (2021) Selective laser melting of Ti6Al4V alloy: process parameters, defects and post-treatments. *J Manuf Process* 64(January):161–187. <https://doi.org/10.1016/j.jmapro.2021.01.009>
- Zhou H et al (2022) Formation and evolution mechanisms of pores in Inconel 718 during selective laser melting: meso-scale modeling and experimental investigations. *J Manuf Process* 81(June):202–213. <https://doi.org/10.1016/j.jmapro.2022.06.072>
- Stavropoulos P, Foteinopoulos P, Papacharalampopoulos A, Tsoukantas G (2019) Warping in SLM additive manufacturing processes: estimation through thermo-mechanical analysis. *Int J Adv Manuf Technol* 104(1–4):1571–1580. <https://doi.org/10.1007/s00170-019-04105-2>
- Mugwagwa L, Dimitrov D, Matope S, Yadroitsev I (2018) Influence of process parameters on residual stress related distortions in selective laser melting. *Procedia Manuf* 21(2017):92–99. <https://doi.org/10.1016/j.promfg.2018.02.099>
- Clijsters S, Craeghs T, Buls S, Kempen K, Kruth JP (2014) In situ quality control of the selective laser melting process using a high-speed, real-time melt pool monitoring system. *Int J Adv Manuf Technol* 75(5–8):1089–1101. <https://doi.org/10.1007/s00170-014-6214-8>
- Mercelis P, Kruth JP (2006) Residual stresses in selective laser sintering and selective laser melting. *Rapid Prototyp J* 12(5):254–265. <https://doi.org/10.1108/13552540610707013>
- Wang D, Yang Y, Yi Z, Su X (2013) Research on the fabricating quality optimization of the overhanging surface in SLM process. *Int J Adv Manuf Technol* 65(9–12):1471–1484. <https://doi.org/10.1007/s00170-012-4271-4>
- Calignano F (2014) Design optimization of supports for overhanging structures in aluminum and titanium alloys by selective laser melting. *Mater Des* 64:203–213. <https://doi.org/10.1016/j.matdes.2014.07.043>
- Bugatti M, Semeraro Q, Colosimo BM (2022) Effect of overhanging surfaces on the evolution of substrate topography and internal defects formation in laser powder bed fusion. *J Manuf Process* 77(March):588–606. <https://doi.org/10.1016/j.jmapro.2022.03.030>
- Lu X, Chiumenti M, Cervera M, Tan H, Lin X, Wang S (2021) Warpage analysis and control of thin-walled structures manufactured by laser powder bed fusion. *Metals (Basel)* 11(5):686. <https://doi.org/10.3390/met11050686>
- Bartlett JL, Li X (2019) An overview of residual stresses in metal powder bed fusion. *Addit Manuf* 27(January):131–149. <https://doi.org/10.1016/j.addma.2019.02.020>
- Kang X, Dong S, Wang H, Yan S, Liu X, Xu B (2020) Inhomogeneous microstructure and its evolution of laser melting deposited 24CrNiMo steel: from single-track to bulk sample. *Mater Sci Eng A* 772(October 2019):138795. <https://doi.org/10.1016/j.msea.2019.138795>
- Bai Y, Zhao C, Wang D, Wang H (2022) Evolution mechanism of surface morphology and internal hole defect of 18Ni300 maraging steel fabricated by selective laser melting. *J Mater Process Technol* 299(July 2021):117328. <https://doi.org/10.1016/j.jmatprotec.2021.117328>
- Wang Y et al (2021) Tuning process parameters to optimize microstructure and mechanical properties of novel maraging steel fabricated by selective laser melting. *Mater Sci Eng A* 823(June):141740. <https://doi.org/10.1016/j.msea.2021.141740>
- Yang J et al (2016) Role of molten pool mode on formability, microstructure and mechanical properties of selective laser melted Ti-6Al-4V alloy. *Mater Des* 110:558–570. <https://doi.org/10.1016/j.matdes.2016.08.036>
- Gusarov AV, Yadroitsev I, Bertrand P, Smurov I (2007) Heat transfer modelling and stability analysis of selective laser melting. *Appl Surf Sci* 254(4):975–979. <https://doi.org/10.1016/j.apsusc.2007.08.074>
- Shrestha S, Chou K (2021) An investigation into melting modes in selective laser melting of Inconel 625 powder: single track geometry and porosity. *Int J Adv Manuf Technol* 114(11–12):3255–3267. <https://doi.org/10.1007/s00170-021-07105-3>
- Kruth JP, Froyen L, Van Vaerenbergh J, Mercelis P, Rombouts M, Lauwers B (2004) Selective laser melting of iron-based powder. *J Mater Process Technol* 149(1–3):616–622. <https://doi.org/10.1016/j.jmatprotec.2003.11.051>
- Gong H, Rafi K, Starr T, Stucker B (2013) The effects of processing parameters on defect regularity in Ti-6Al-4V parts fabricated by Selective Laser Melting and Electron Beam Melting. 24th Int SFF Symp - An Addit Manuf Conf SFF 2013:424–439
- Song B, Dong S, Zhang B, Liao H, Coddet C (2012) Effects of processing parameters on microstructure and mechanical property of selective laser melted Ti6Al4V. *Mater Des* 35:120–125. <https://doi.org/10.1016/j.matdes.2011.09.051>
- Costa A, Buffa G, Palmeri D, Pollara G, Fratini L (2022) Hybrid prediction-optimization approaches for maximizing parts density in SLM of Ti6Al4V titanium alloy. *J Intell Manuf* 33(7):1967–1989. <https://doi.org/10.1007/s10845-022-01938-9>
- Balaa M, Mekhiel S, Elbestawi M, McIsaac J (2020) On selective laser melting of Inconel 718: densification, surface roughness, and residual stresses. *Mater Des* 193:108818. <https://doi.org/10.1016/j.matdes.2020.108818>
- Yadroitseva I, Els J, Booyens G (2015) Peculiarities of single track formation from ti6al4v alloy at different laser power densities by selective laser melting. *S Afr J Ind Eng* 26(3):86–95. <https://doi.org/10.7166/26-3-1185>
- Lu P, Cheng-Lin Z, Liang W, Tong L, Jiang-Lin L (2020) Molten pool structure, temperature and velocity flow in selective laser melting AlCu5MnCdVA alloy. *Mater Res Express* 7(8):086516. <https://doi.org/10.1088/2053-1591/abadcf>
- Qiu C, Panwisawas C, Ward M, Basoalto HC, Brooks JW, Attallah MM (2015) On the role of melt flow into the surface structure

- and porosity development during selective laser melting. *Acta Mater* 96:72–79. <https://doi.org/10.1016/j.actamat.2015.06.004>
30. Yin J et al (2020) Correlation between forming quality and spatter dynamics in laser powder bed fusion. *Addit Manuf* 31(November 2019):100958. <https://doi.org/10.1016/j.addma.2019.100958>
31. Zhang T et al (2019) Evolution of molten pool during selective laser melting of Ti-6Al-4V. *J. Phys D Appl Phys* 52(5):055302. <https://doi.org/10.1088/1361-6463/aaee04>

**Publisher's Note** Springer Nature remains neutral with regard to jurisdictional claims in published maps and institutional affiliations.